The Seventh Asian-Pacific Symposium on Structural Reliability and Its Applications (APSSRA2020)
October 4–7 2020, Tokyo, Japan
T. Takada, I. Yoshida & T. Itoi (editors)

Seismic Fragility Analysis of Human Injury Using Seismic Response Analysis Model of Human Bodies

Y. Matsumoto[1], T. Hida[2], T. Takada[3] and T. Itoi[4]

[1]*Graduate Student, School of Engineering, The University of Tokyo. Email: matsumoto@load.arch.t.u-tokyo.ac.jp*
[2]*Assistant Professor, School of Engineering, The University of Tokyo. Email: hida@load.arch.t.u-tokyo.ac.jp*
[3]*Director, Office for Promotion of Risk-informed Applications, Nuclear Safety and Disaster Prevention Support Section, Japan Atomic Energy Agency. Email: takada.tsuyoshi@jaea.go.jp*
[4]*Associate Professor, School of Engineering, The University of Tokyo. Email: tatsuya.itoi@arch.t.u-tokyo.ac.jp*

Abstract: Human casualties frequently occur during strong earthquake motions, and the seismic response analysis model of human bodies is useful for quantitatively evaluating human injuries owing to those earthquake shakings. In this study, response analyses of human bodies were conducted, considering the variations of individual differences and input ground motion characteristics. From the analysis results, the input motion parameters adequately required to estimate the human response to earthquake shaking were identified, and fragility curves of human injury were plotted. Individual differences should be considered in evaluating human injuries due to earthquakes.

Keywords: indoor safety, human injury, fragility curve, response analysis, feedback control

1. Introduction

The consideration of indoor safety during severe earthquakes is necessary to minimize casualties in buildings caused by falling of flying objects and being knocked down, in addition to casualties owing to building collapse. Most human casualties occur as injuries, such as bruises caused by overturning of furniture or cuts by broken glass. However, injuries from the seismic response of humans, for example, being knocked down by earthquake shaking or the collision of the head to the wall, also occur (Tokyo Fire Department, 2016).

Human safety during earthquakes should also be considered for emergency response after an earthquake. When a severe earthquake occurs, people should manage the emergency to mitigate the consequences of the disaster. A typical example is accident management at the time of the Fukushima Daiichi Nuclear Power Plant accident in 2011 caused by tsunami that followed the 2011 off the Pacific coast of Tohoku Earthquake.

In Japan, anticipating and managing seismic risk that in not well understood, including mega earthquakes such as the Nankai Trough earthquake, is a significant issue. The evaluation of structural safety under such earthquakes shaking is frequently conducted. However, how such earthquake shaking affects the human body is unclear. Damage estimation methodology and measures to minimize human casualties should be proposed and explained.

Most previous studies on indoor human damages during an earthquake focused on casualties caused by the overturning of furniture, and the behavior of the human body is usually ignored. Some studies considered human behavior during earthquake shaking, but the human response to earthquake motions was not assessed. Hence, it is essential to evaluate the seismic response of human bodies to predict indoor damages to humans accurately. Shaking table tests are useful for assessing the behavior of building structures under earthquake shaking. However, it is impossible to conduct shaking table tests to investigate the seismic response of humans to severe earthquake motions. Thus, the seismic response analysis model of human bodies is valuable for evaluating human behavior during such earthquakes.

Previous studies (Hida et al., 2019; Matsumoto et al., 2020) proposed seismic response analysis models of the human body based on shaking table test results. When investigations on human damages under earthquake shaking are conducted, person-to-person differences are considered critical. In this study, the seismic fragility analysis of human bodies inputting various strong motion records was conducted for two different human objects to investigate the need to consider person-to-person differences. First, the relationship between the characteristics of input motions and the seismic response of humans was established. Then, fitting parameters of the input motion were identified to estimate the human response. Finally, the fragility curve of human injury caused by hitting the head on the wall was evaluated by introducing the head injury criterion (HIC) score (Michael et al., 1998), which is a measure of head injury.

2. Model and analysis conditions

2.1 Seismic response analysis model of human bodies

A cart-type double inverted pendulum, depicted in Figure 1, is adopted as the seismic response analysis model for the behavior in the front-back direction of human bodies. In this model, Pendulums 1 and 2 correspond to upper and lower parts of human body, respectively. The posture control of the human body to shaking is modeled as the feedback control to the pendulum, which ensures that the pendulums do not fall over during shaking. Table 1 lists the symbols used in the model and their respective descriptions.

Table 1. Symbols used for cart-type double inverted pendulum shown in Figure 1

Symbol	Description
$\xi_0(t)$	Absolute displacement of the floor
$\xi(t)$	Relative displacement of the cart to with respect to the floor
$\theta_1(t)$	Angle of Pendulum 1
$\theta_2(t)$	Angle of Pendulum 2
$f_c(t)$	Control force applied to the cart
$\tau(t)$	Joint torque between Pendulum 1 and 2
m_1	Mass of Pendulum 1
m_2	Mass of Pendulum 2
m_c	Cart mass
L_1	Length of Pendulum 1
L_2	Length of Pendulum 2
l_1	Length from the lower tip to the center of gravity of Pendulum 1
l_2	Length from the lower tip to the center of gravity of Pendulum 2
J_1	Moment of inertia of Pendulum 1
J_2	Moment of inertia of Pendulum 2
D_1	Time delay of the control system
D_2	Time delay for ξ(t)
μ_c	Viscous damping coefficient of cart (= 10000 Ns/m)
g	Gravity acceleration (= 9.806 m/s^2)
$\mathbf{K}_{fc}$	Vector of feedback gains about $f_c(t)$
$\mathbf{K}_\tau$	Vector of feedback gains about $\tau(t)$
$\mathbf{x}(t)$	Vector of state variables

Table 2. Information of subjects

-	subject B	subject C
sex	male	male
age	23	22
height (cm)	169	167
weight (kg)	51	57

Table 3. Parameters of model (Matsumoto et al., 2020)

-	Subject B	Subject C
m_1 (kg)	14.9	16.7
m_2 (kg)	34.6	38.6
m_c (kg)	1.50	1.68
L_1 (m)	0.830	0.820
L_2 (m)	0.794	0.785
l_1 (m)	0.459	0.453
l_2 (m)	0.305	0.301
J_1 (kgm^2)	5.10	5.55
J_2 (kgm^2)	3.21	3.50

2.2 Equation of motion and control system of model

The equation of motion of the model obtained using the Euler-Lagrange equation is expressed as follows:

$$\begin{aligned} &d_1\left(\ddot{\xi}_0(t)+\ddot{\xi}(t)\right)+d_2\ddot{\theta}_1(t)\cos\theta_1(t)\\ &+d_3\ddot{\theta}_2(t)\cos\theta_2(t)-d_2\{\dot{\theta}_1(t)\}^2\sin\theta_1(t)\\ &\qquad -d_3\{\dot{\theta}_2(t)\}^2\sin\theta_2(t)+\mu_c\dot{\xi}(t)=f_c(t)\end{aligned} \tag{1}$$

$$\begin{aligned} &d_2\left(\ddot{\xi}_0(t)+\ddot{\xi}(t)\right)\cos\theta_1(t)+d_4\ddot{\theta}_1(t)\\ &+d_5\ddot{\theta}_2(t)\cos(\theta_1(t)-\theta_2(t))-d_7\sin\theta_1(t)\\ &\qquad +d_5\{\dot{\theta}_2(t)\}^2\sin(\theta_1(t)-\theta_2(t))=-\tau(t)\end{aligned} \tag{2}$$

$$\begin{aligned} &d_3\left(\ddot{\xi}_0(t)+\ddot{\xi}(t)\right)\cos\theta_2(t)+d_6\ddot{\theta}_2(t)\\ &+d_5\ddot{\theta}_1(t)\cos(\theta_1(t)-\theta_2(t))-d_8\sin\theta_2(t)\\ &\qquad -d_5\{\dot{\theta}_1(t)\}^2\sin(\theta_1(t)-\theta_2(t))=\tau(t)\end{aligned} \tag{3}$$

where,

$$\begin{aligned} &d_1=m_1+m_2+m_c \quad && d_2=m_1l_1+m_2l_2\\ &d_3=m_2l_2 && d_4=m_1{l_1}^2+m_2{L_1}^2+J_1\\ &d_5=m_2l_2L_1 && d_6=m_2{l_2}^2+J_2\\ &d_7=m_1l_1g+m_2L_1g && d_8=m_2l_2g\end{aligned} \tag{4}$$

A feedback control system is adopted for modeling the posture control of humans. The block diagram shown in Figure 2 describes the control system of the model.

In this model, Pendulums 1 and 2 are controlled to maintain the standing posture by generating control forces for making each of the elements of the state variable $\mathbf{x}(t)$, except for $\xi(t)$, equal to zero. A time lag in human reaction,

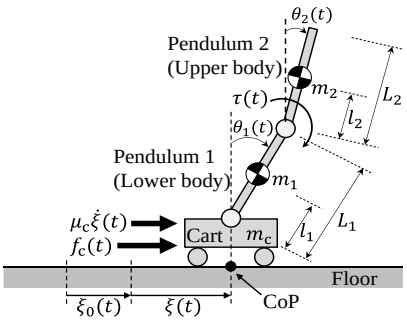

Figure 1. The cart type double inverted pendulum

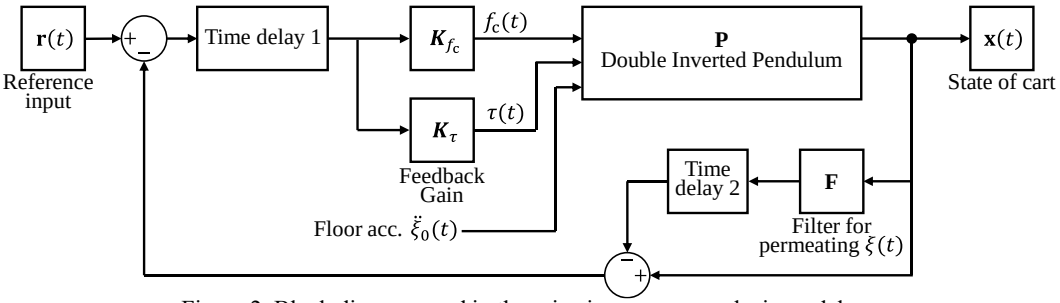

Figure 2. Block diagram used in the seismic response analysis model

Table 4. Feedback gains (Matsumoto et al., 2020)

	Subject B	Subject C
$k_{f\xi}$	3000	7190
$k_{f\theta_1}$	-78200	-37400
$k_{f\theta_2}$	-20100	-16000
$k_{f\dot{\xi}}$	-11300	-14500
$k_{f\dot{\theta}_1}$	-17800	-15100
$k_{f\dot{\theta}_2}$	-6510	-4600
$k_{\tau\xi}$	-54.6	-61.6
$k_{\tau\theta_1}$	-89.0	19.3
$k_{\tau\theta_2}$	119	183
$k_{\tau\dot{\xi}}$	-16.8	-24.1
$k_{\tau\dot{\theta}_1}$	-27.8	-25.4
$k_{\tau\dot{\theta}_2}$	28.7	32.9

which is considered to correspond to the time required for the human body not to react to any input, is also considered in this model. Therefore, the time lag is considered as the dead time of the control system, and then controlling forces $f_c(t)$ and $\tau(t)$ are calculated as follows:

$$f_c(t) = -\mathbf{K}_{f_c}\mathbf{x}(t - D_1) \quad (5)$$

$$\tau(t) = -\mathbf{K}_{\tau}\mathbf{x}(t - D_1) \quad (6)$$

where,

$$\mathbf{x}(t) = \left[\xi(t) \quad \theta_1(t) \quad \theta_2(t) \quad \dot{\xi}(t) \quad \dot{\theta}_1(t) \quad \dot{\theta}_2(t)\right]^{\mathrm{T}} \quad (7)$$

$$\mathbf{K}_{f_c} = \left[k_{f\xi} \quad k_{f\theta_1} \quad k_{f\theta_2} \quad k_{f\dot{\xi}} \quad k_{f\dot{\theta}_1} \quad k_{f\dot{\theta}_2}\right] \quad (8)$$

$$\mathbf{K}_{\tau} = \left[k_{\tau\xi} \quad k_{\tau\theta_1} \quad k_{\tau\theta_2} \quad k_{\tau\dot{\xi}} \quad k_{\tau\dot{\theta}_1} \quad k_{\tau\dot{\theta}_2}\right] \quad (9)$$

Subsequently, the state variable $\mathbf{x}(t)$ is obtained by substituting $f_c(t)$, and $\tau(t)$ of Eqs. (5) and (6), and the input acceleration $\ddot{\xi}_0(t)$ into Eqs. (1) ~ (3).

We use two models for the human subjects, named Subject B and Subject C models, as the seismic response analysis model of different human bodies. The parameters for these models were obtained to replicate the seismic responses of Subjects B and C based on shaking table tests that were performed in 2017 and 2018 (Hida et al., 2019). Tables 2 and 3 list the information of Subjects B and C and the parameters originating from the weights and heights of Subjects B and C. The values of the parameters are obtained by calculating the length and the weight of some part of each subjects' body referring to the segment length between any joints in the human body (Winter, 2009) and the inertia coefficient of the body segments (Robertson et al., 2013). Table 4 lists the feedback gains of the control system obtained for each human subject (Matsumoto et al., 2020). These models are validated using the results of the shaking table tests and are considered to yield reasonable results for other types of input motions. Nevertheless, they were validated only for a few test results. The applicability of the models concerning the analysis of the various seismic motion types, particularly for those with high amplitudes, was not confirmed fully.

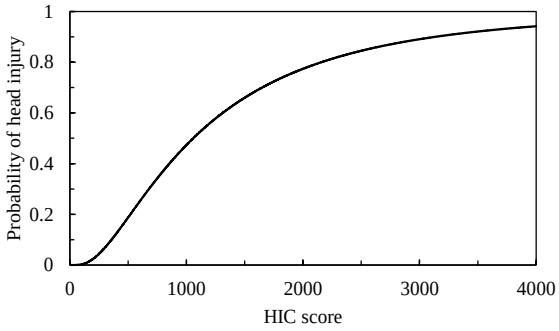

Figure 3. HIC score and probability of injury (Michael et al. 1998)

2.3 Evaluation method of human injury

In this study, the HIC score (Michael et al., 1998) is used to evaluate human injury quantitatively. The HIC score, which was proposed by National Highway Traffic Safety Administration (NHTSA) in cases where the head collides with an object, indicates the severity of head injury. The HIC score is defined as follows:

$$HIC = \max\left\{\frac{1}{t_2 - t_1}\int_{t_1}^{t_2} a(t)\mathrm{d}t\right\}^{2.5}(t_2 - t_1) \quad (10)$$

where t_1 and t_2 are any two arbitrary times during the acceleration pulse, and $a(t)$ is the acceleration of the head during the collision.

In calculating the HIC score from the results of the seismic response analysis of human bodies, it is assumed that the acceleration of the head during the collision is constant. Hence, the following equation is obtained by rearranging Eq. (10) (Ito et al., 2020), as follows:

$$HIC = \left\{\frac{V_0}{g\Delta t}(1 + e)\right\}^{2.5}\Delta t \quad (11)$$

where V_0 is the relative velocity of the head with respect to the colliding object, e is the restitution coefficient, and Δt is the collision time. Each parameter was determined, assuming that the head collided with the surface of the rigid body at its maximum velocity. Note that this assumption could overestimate the head injury. We obtained e = 0.4 and Δt = 0.0027 s.

The seismic response velocity of the human head is obtained as the relative velocity of the head of Pendulum 2 with respect to the floor and is determined as follows:

$$\dot{\xi}_{\mathrm{head}}(t) = \dot{\xi}(t) + L_1\dot{\theta}_1(t)\cos\theta_1(t) + L_2\dot{\theta}_2(t)\cos\theta_2(t) \quad (12)$$

Therefore, V_0 is obtained as follows:

$$V_0 = \max\{\dot{\xi}_{\mathrm{head}}(t)\} \quad (13)$$

Figure 3 shows the relationship between the HIC score and the probability of skull fracture, P, proposed by Michael et al. (1998). The probability is expressed as follows:

$$P = \Phi\left(\frac{\ln(HIC) - \mu}{\sigma}\right) \tag{14}$$

where Φ is the cumulative distribution function of the standard normal distribution, μ is the logarithmic mean (= 6.96) and σ is the logarithmic standard deviation (= 0.847).

In this study, the non-exceedance probability curve of the HIC score is assumed to be the "capacity" of human body and the fragility curve of human body is obtained as a function of the maximum velocity of input earthquake motions V_{max} by transforming the variable of the capacity from the HIC score to V_{max}.

2.4 Input earthquake motion and analysis conditions

The strong motion records of K-NET (National Research Institute for Earth Science and Disaster Resilience, 2019) observed during the four earthquakes listed in Table 5 are used for input earthquake motions to human subjects. The four earthquakes are denoted as follows: The Western Tottori prefecture earthquake in 2000 (I), The Niigataken Chuetsu-oki Earthquake in 2007 (II), The 2011 off the Pacific coast of Tohoku Earthquake (III), and The 2016 Kumamoto Earthquake (IV). Figure 4 shows the locations of the epicenter and observation stations for each earthquake.

Assuming that each human subject is exposed to the earthquake motion at ground level, the observed strong motion records are used as the input in the model. The response analyses are conducted using both the Subject B and C models. As discussed in Section 2.1, the model used in this study is a one-dimensional model that simulated the behavior in the front-back direction of the human body. Subsequently, the geometrical mean of the results of the response analysis for the north-south and east-west components of each grand motion record is used. It should be noted that the observed records are directly used as input earthquake motions in this study; the results may be different when the floor response of the building is adopted as the human model input.

3 Analysis results and discussion

3.1 Input ground motion and human response

The relationship between the maximum acceleration of the input earthquake motion and the maximum head response velocity of Subjects B and C is determined (Figure 5) to investigate the relationship between the characteristics of the input motion and human response. The relationship between the maximum velocity of the input earthquake motion and the maximum head response velocity of Subjects B and C is shown in Figure 6. The maximum velocity of the input earthquake motion and the maximum head response velocity have a higher positive correlation compared to the maximum acceleration of the input motion. Therefore, the maximum velocity of the input motion can be regarded as a suitable indicator for estimating the human response.

3.2 Evaluation formula for human injury

Seismic fragility curves for Subjects B and C are derived to evaluate the injury of subjects and to determine the

Table 5. List of earthquakes of input motions

-	I	II	III	IV
Date	10/6/'00	7/16/'07	3/11/'11	4/16/'16
Time	13:30	10:13	14:46	1:25
Epicenter	35.3°N 133.3°E	37.6°N 138.6°E	38.1°N 142.9°E	32.8°N 130.8°E
Depth	11 km	17 km	24 km	12 km
Mw	6.6	6.6	9.0	7.0

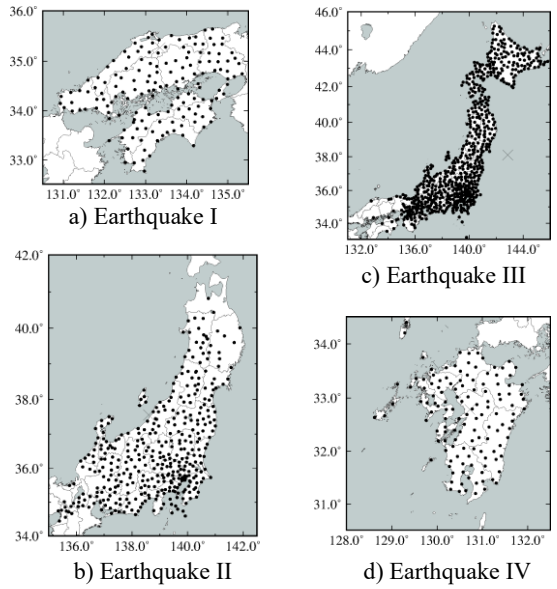

Figure 4. Location of epicenter and observation points

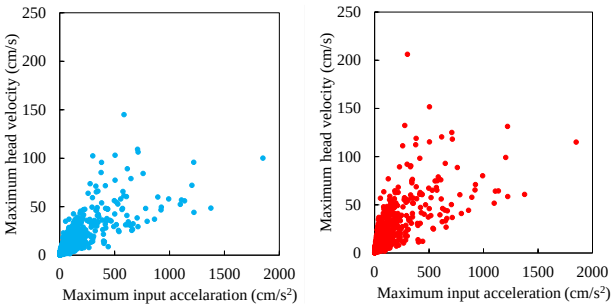

Figure 5. Max. input acceleration and max. head velocity

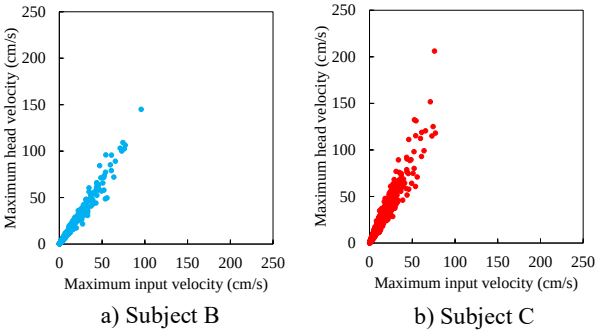

Figure 6. Max. input velocity and max. head velocity

person-to-person difference in human behavior during an earthquake. First, a regression analysis is conducted using the results presented in Figure 6, and the following equations, which express the relationships between the maximum velocity of the input motion and the maximum head response velocity of Subjects B and C, are obtained:

$$\ln(v_{\mathrm{B\,max}}) = 0.992 \cdot \ln(V_{\max}) + 0.289 \tag{15}$$

$$\ln(v_{\mathrm{C\,max}}) = 1.002 \cdot \ln(V_{\max}) + 0.574 \tag{16}$$

where $V_{\max}$ is the maximum velocity of the input motion, and $v_{\mathrm{B\,max}}$ and $v_{\mathrm{C\,max}}$ are the maximum head velocities of Subjects B and C, respectively. The regression lines are displaced in Figure 7. The standard deviations $\sigma_{1\mathrm{B}}$ and $\sigma_{1\mathrm{C}}$ of the residuals in Eqs. (15) and (16) are obtained as follows:

$$\sigma_{1\,B} = 0.106 \qquad \sigma_{1\,C} = 0.200 \tag{17}$$

By rearranging Eq. (11), the following equation for the HIC score is obtained, as follows:

$$\ln(HIC) = 2.5 \ln V_0 + \ln\left[\left(\frac{1+e}{g\Delta t}\right)^{2.5} \Delta t\right] \tag{18}$$

From Eqs. (15) and (16), V_0 is determined as follows:

$$\ln V_0 = a \ln(V_{\max}) + b + E_1 \tag{19}$$

where a and b are the regression coefficients, and E_1 is a random variable for the regression residual that follows the normal distribution with a zero mean and a standard deviation of σ_1. Then, Eq. (19) is substituted into Eq. (18).

$$\ln(HIC) = 2.5\left\{a \ln(V_{\max}) + b + E_1\right\} + \ln\left[\left(\frac{1+e}{g\Delta t}\right)^{2.5} \Delta t\right] \tag{20}$$

By rearranging Eq. (20), $V_{\max}$ is determined and expressed using the following equation.

$$\ln(V_{\max}) = \frac{\ln(HIC)}{2.5a} - \frac{1}{2.5a} \ln\left[\left(\frac{1+e}{g\Delta t}\right)^{2.5} \Delta t\right] - \frac{b}{a} - \frac{E_1}{a} \tag{21}$$

From Eq. (14), $V_{\max}$ is finally determined as follows:

$$\ln(V_{\max}) = \frac{\mu}{2.5a} - \frac{1}{2.5a} \ln\left[\left(\frac{1+e}{g\Delta t}\right)^{2.5} \Delta t\right] - \frac{b}{a} - \frac{E_1}{a} + \frac{E_2}{2.5a} \tag{22}$$

where E_2 is a random variable following a normal distribution with a zero mean and a standard deviation of σ that corresponds to the probability distribution of injury in Eq. (14). Thus, the probability of head injury P is determined as a function of the input velocity, as follows:

$$P = \Phi\left(\frac{\ln(V_{\max}) - \mu'}{\sigma'}\right) \tag{23}$$

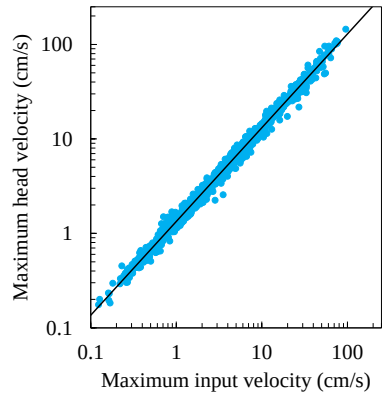

a) Subject B

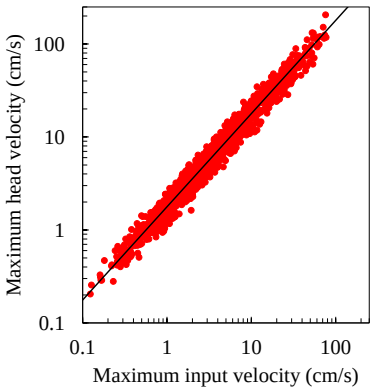

b) Subject C

Figure 7. Regression line

where the probability of head injury follows the log-normal distribution, and its logarithmic mean μ' and logarithmic standard deviation σ' are expressed as follows:

$$\mu' = \frac{\mu}{2.5a} - \frac{1}{2.5a} \ln\left[\left(\frac{1+e}{g\Delta t}\right)^{2.5} \Delta t\right] - \frac{b}{a} \tag{24}$$

$$\sigma' = \sqrt{\left(\frac{\sigma_1}{a}\right)^2 + \left(\frac{\sigma_2}{2.5a}\right)^2} \tag{25}$$

3.3 Probability of head injury in Subjects B and C

The probabilities of head injury for Subjects B and C are determined using Eqs. (15) and (16). First, from e = 0.4, g = 980.6 cm/s^2, and Δt = 0.0027 s, the following equation is determined:

$$\ln\left[\left(\frac{1+e}{g\Delta t}\right)^{2.5} \Delta t\right] \approx -7.5075 \tag{26}$$

Then, from Eqs. (15), (16), and (18), the HIC scores for Subjects B and C are obtained as a function of $V_{\max}$, as follows:

$$\ln(HIC_{\mathrm{B}}) = 2.480 \cdot \ln(V_{\max}) - 6.785 \tag{27}$$

$$\ln(HIC_{\mathrm{C}}) = 2.505 \cdot \ln(V_{\max}) - 6.073 \tag{28}$$

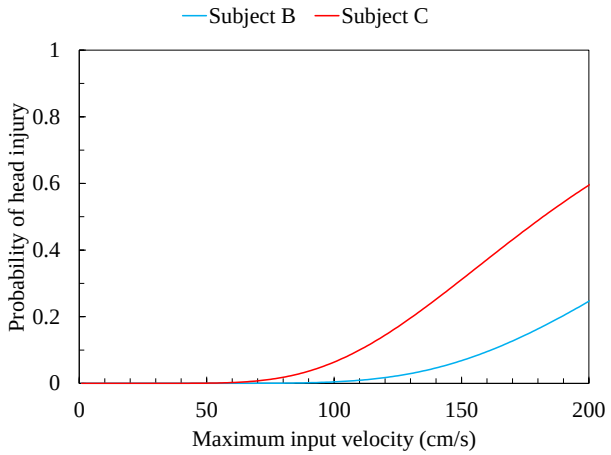

Figure 8. Fragility curve of subject B and C

where HIC_B and HIC_C are the HIC scores of Subjects B and C, respectively. The μ' and σ' values of each subject are calculated using Eqs. (24) and (25), as follows.

$$\mu'_B = 5.544 \qquad \mu'_C = 5.204$$
$$\sigma'_B = 0.358 \qquad \sigma'_C = 0.393$$

The probabilities of head injury for Subject B and C are finally determined as follows.

$$P_B = \Phi\left(\frac{\ln(V_{max}) - 5.544}{0.358}\right) \tag{29}$$

$$P_C = \Phi\left(\frac{\ln(V_{max}) - 5.204}{0.393}\right) \tag{30}$$

Figure 8 shows the fragility curves of the head injury of Subjects B and C as a function of the maximum velocity of the input motion. From Figure 8, the probability of injury of Subject C is higher than that of Subject B. For example, when the maximum velocity of the input motion is 150 cm/s, the probabilities of head injury of Subject B and C are 0.068 and 0.311, respectively; the probability of head injury of Subject C is approximately five times higher than that of Subject B. Considering that Subjects B and C are similar, i.e., both are males in their 20s, a more significant difference could be observed when the probabilities of injury of several people are considered, including older adults, who are considered to have a higher possibility of being knocked down than younger people.

A conservative assumption, however, was made when calculating the HIC score using Eq. (11), so there was a possibility that the severity of the head injury was evaluated conservatively. Considering the actual conditions of Subjects B and C during the shaking table tests that Subject C managed better than Subject B, the results presented in Figure 8 have opposite tendencies. One of the reasons for this trend is that human injury owing to earthquake shaking is not limited to collision, and other causes of injury, therefore, should also be considered.

4 Conclusions

In this study, seismic response analyses, in which various types of strong motion records were input, was conducted using the seismic response analysis model of human bodies. It was shown that the maximum velocity of the input motion was a suitable index for assessing the severity of the human response, i.e., the head velocity owing to an earthquake. Next, the fragility curves of head injury were obtained as a function of the maximum velocity of the earthquake motion to determine the person-to-person variability of injury owing to earthquake motions. The fragility curve showed that there was a significant difference between the subjects, and consideration of person-to-person differences in human injury is critical. The proposed model is useful for quantitatively assessing such human injury.

Acknowledgement

Strong motion records used in this study were provided by NIED K-NET, National Research Institute for Earth Science and Disaster Resilience. This study was supported by JSPS KAKENHI Grant Number JP19H02339.

References

Tokyo Fire Department. 2016. Result of Research on the Actual Situation about Indoor Damage due to the 2016 Kumamoto Earthquake. (In Japanese)

Hida, T., Ohno, A., Itoi, T., Takada, T. 2019. Development of Seismic Response Analysis Model of Human Body by Cart-type Double Inverted Pendulum Model for Prediction of Human Injury During Earthquake. In *Journal of Structure and Construction Engineering* (Transactions of AIJ), Vol. 84, No. 765, pp. 1377-1387. (In Japanese with English abstract)

Matsumoto, Y., Hida, T., Takada, T., Itoi, T. 2020. Development of Nonlinear Seismic Response Analysis Model of Human Body Considering Individual Differences. *In Summaries of technical papers of annual meeting Architecture Institute of Japan*. (In Japanese)

Michael, K., Emily, S., Rolf, E., Shashi, K. and Roger, S. 1998. Development of improved injury criteria for the assessment of advanced automotive restraint systems.

Winter, D.A. 2009. Biomechanics and Motor Control of Human Movement, 4th Edition.

Robertson, D. Gordon E., Caldwell, Graham E., Hamill, Joseph, Kamen, Gray, Whittlesey, Saunders N. 2013. Research Methods in BIOMECHANICS, 2nd Edition.

Ito, K., Hida, T., Itoi, T. and Takada, T. 2020. Development of Evaluation Methodology of Human Injury During Earthquake Based on Seismic Response Analysis Model of Human Body. In *Journal of Structure and Construction Engineering* (Transactions of AIJ), Vol. 85, No. 767, pp. 159-168. (In Japanese with English abstract, figures and tables)

National Research Institute for Earth Science and Disaster Resilience. 2019. NIED K-NET, National Research Institute for Earth Science and Disaster Resilience.